Correlations of Rydberg excitations in an ultracold gas after an echo sequence

S. Wüster,[1,*] J. Stanojevic,[1] C. Ates,[1] T. Pohl,[1] P. Deuar,[2] J. F. Corney,[3] and J. M. Rost[1]

[1]*Max Planck Institute for the Physics of Complex Systems, Nöthnitzer Strasse 38, D-01187 Dresden, Germany*

[2]*Institute of Physics, Polish Academy of Sciences, Aleja Lotników 32/46, PL-02-668 Warsaw, Poland*

[3]*ARC Centre of Excellence for Quantum-Atom Optics, School of Mathematics and Physics, University of Queensland, Brisbane, QLD 4072, Australia*

(Received 4 November 2009; published 8 February 2010)

We show that Rydberg states in an ultracold gas can be excited with strongly preferred nearest-neighbor distance if densities are well below saturation. The scheme makes use of an echo sequence in which the first half of a laser pulse excites Rydberg states while the second half returns atoms to the ground state, as in the experiment of Raitzsch *et al.* [Phys. Rev. Lett. **100**, 013002 (2008)]. Near the end of the echo sequence, almost any remaining Rydberg atom is separated from its next-neighbor Rydberg atom by a distance slightly larger than the instantaneous blockade radius halfway through the pulse. These correlations lead to large deviations of the atom-counting statistics from a Poissonian distribution. Our results are based on the exact quantum evolution of samples with small numbers of atoms. Finally, we demonstrate the utility of the ω expansion for the approximate description of correlation dynamics through an echo sequence.

DOI: 10.1103/PhysRevA.81.023406 PACS number(s): 32.80.Ee, 32.80.Rm, 34.20.Cf

I. INTRODUCTION

When atoms within an ultracold gas are excited to Rydberg levels, they experience long-range interactions that can block further excitations, leading to a strongly correlated many-body state. This effect might be useful for quantum information [1] as well as for fundamental studies of many-body physics and was observed in several experiments [2–11]. The coherence of the excitation process in a bulk gas has been experimentally demonstrated using an echo technique [8,9]. After exciting atoms to Rydberg states, it was possible to deexcite them following a π phase shift of the excitation laser. The basic scheme is illustrated in Fig. 1. After the echo sequence, a certain fraction of the atoms remains in the excited state, owing to effects of the interaction. This has been modeled theoretically using the super-atom approach [12].

Neither experiment nor theory has considered the dynamics of Rydberg-Rydberg correlations during such an echo sequence. Here, we show that strong correlations of atoms separated by a characteristic distance r_0 are induced in its course. This distance r_0 is slightly larger than the instantaneous blockade radius at the moment when the laser phase is flipped. At the instantaneous blockade radius $r_b(t)$, the Rydberg state density-density correlation function drops sharply to zero. Initially, $r_b(t) = 0$, later growing toward its saturation value $r_{b0} \sim (C_6/\Omega)^{1/6}$, as the longer duration of the pulse allows an increasingly finer energy resolution.

After most Rydberg atoms that were excited in the first half of the pulse return to the ground state, the majority of the remainder are between r_0 and $1.5r_0$ from their nearest excited neighbor. The strength of this correlation signal is proportional to ρ^{-2}, where ρ is the atomic density.

Our results imply that the echo technique can be used to manipulate the nearest-neighbor distribution in the Rydberg fraction of the gas. Such manipulations could be used, for example, to initiate dynamics due to dipole-dipole forces [13] from a well-specified nonequilibrium state.

Similar correlations between Rydberg atoms are created if a two-step excitation scheme with a strongly decaying intermediate state is used [14,15]. In that case they are due to the Autler-Townes splitting of the intermediate level.

The peculiar nature of the nearest-neighbor distribution function of Rydberg atoms after an echo pulse may be seen experimentally in the kinetic energy spectrum of ions after field ionization of the remaining Rydberg fraction. Alternatively one could measure deviations of the atom-counting statistics from a Poissonian distribution [16]. Both these suggestions are discussed further in Sec. IV.

Our results are based on solutions of the many-particle Schrödinger equation, which we also use to benchmark the recently proposed ω expansion [17,18]. Both methods are briefly described in Sec. II. The ensuing correlation dynamics are presented in Sec. III. Possible ways to detect the pairing effect are discussed in Sec. IV. In Sec. V, we take a closer look at the effects of density variations on our results, and in Sec. VI we directly compare many-body quantum simulations with the ω expansion. Finally, we conclude in Sec. VII.

II. METHODS

A. Exact quantum dynamics

We consider a system of N_0 atoms at fixed locations x_i and described by the following Hamiltonian in atomic units:

$$\hat{H} = \frac{1}{2}\sum_{i=1}^{N_0} \Omega w(t)\left(\sigma_{eg}^i + \sigma_{ge}^i\right) + \Delta \sum_{i=1}^{N_0} \sigma_{ee}^i + \sum_{i,j;j>i}^{N_0} \kappa_{ij}\sigma_{ee}^i\sigma_{ee}^j. \tag{1}$$

Each atom can either be in its ground state $|g\rangle$ or an excited state $|e\rangle$, which is the Rydberg state. The atoms in $|e\rangle$ experience long-range interactions $\kappa_{ij} = -C_6/|x_i - x_j|^6$. Laser-induced transitions between the levels occur with Rabi frequency $\Omega \in \mathbb{R}$, detuning Δ, and the temporal profile of

*sew654@pks.mpg.de

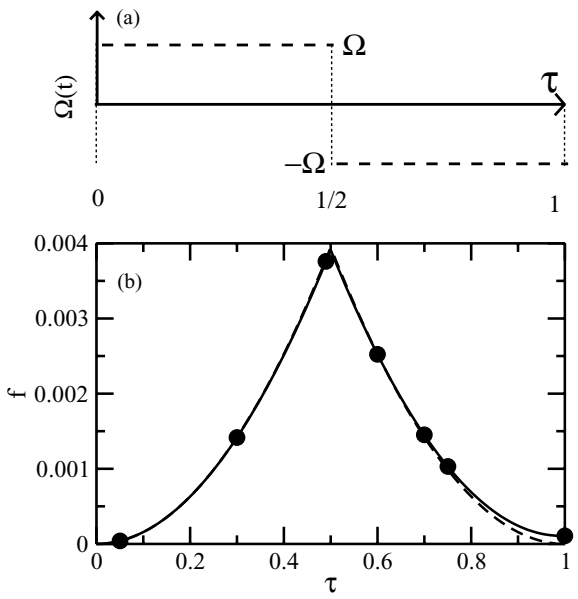

FIG. 1. Illustration of an echo excitation sequence and evolution of the Rydberg fraction. For a sequence of duration T, we use the fractional time $\tau = t/T$. (a) Sketch of Rabi frequency $\Omega w(t)$ (see Sec. II A) during the sequence. (b) Fraction of excited state atoms f for a density $\rho_0 V_{b0} = 26.2$ (solid line) from a numerical solution of the Schrödinger equation. Here, $V_{b0} = 4\pi r_{b0}^3/3$ is a simple estimate of the saturated blockade volume. We also show the noninteracting result for the excited fraction (dashed line). The symbols (•) mark times for which we display correlations in Fig. 2.

the pulse $w(t)$. The operators σ_{ab}^i act as $\sigma_{ab}^i = |a\rangle\langle b|$ on the subspace of atom i and as unity on others. We use atomic units unless otherwise indicated.

We expand the many-body wave function as $|\Psi(t)\rangle = \sum_{\mathbf{n}} c_{\mathbf{n}}|\mathbf{n}\rangle$, where $\mathbf{n}$ is a vector with N_0 elements $n_j \in \{0, 1\}$, which describe whether atom j is in the ground (0) or excited (1) state. The Schrödinger equation (SE) then takes the form

$$i\dot{c}_{\mathbf{n}} = \left(\Delta \sum_i^{N_0} n_i + \sum_{i,j;i>j}^{N_0} \kappa_{ij} n_i n_j\right) c_{\mathbf{n}} + \frac{1}{2}\sum_i^{N_0} [\Omega w(t) c_{\mathbf{n},\downarrow i} + \Omega^* w^*(t) c_{\mathbf{n},\uparrow i}], \quad (2)$$

where $c_{\mathbf{n},\downarrow i}$ ($c_{\mathbf{n},\uparrow i}$) is the coefficient of the state that is reached from $|\mathbf{n}\rangle$ by lowering (raising) the ith atom if this is possible, and 0 otherwise.

For the numerical solution we convert Eq. (2) to a rotating frame for the variables

$$\tilde{c}_{\mathbf{n}} = \exp\left(-it \sum_{i,j;i>j}^{N_0} \kappa_{ij} n_i n_j\right) c_{\mathbf{n}}. \quad (3)$$

To render simulations of ensembles with hundreds of atoms possible, we remove all states whose interaction energy is larger than some cutoff E_{cut} from the Hilbert space (see, e.g., [19,20]). We further limit the number of simultaneously excited atoms to $\sum n_j \leqslant N_{\max}$. All numerical results are checked for convergence with respect to variations in $N_{\max}$ and E_{cut}.

B. The ω expansion

In the experiment of Ref. [8], the sign of the Rabi coupling was flipped well before the excitation of Rydberg atoms reached the saturation limit imposed by the blockade effect. In such a situation one could attempt to solve the quantum dynamics of the gas by a series expansion in $\omega = \Omega t$ [17], where $\omega = 0.25$ for the experimental conditions.

From Eq. (1), we can derive equations of motion for the operators σ_{ab}^i. We expand these operators in a series $\sigma_{ab}^i = \sum_n \omega^n \sigma_{ab}^{i(n)}$. It is possible to obtain recursive equations expressing $\sigma_{ab}^{i(n)}$ by $\sigma_{a'b'}^{i(m)}$ for $m < n$. In our case the lowest order approximations of the σ_{ab}^i already offer interesting insight into correlation dynamics.

In the following we are interested in an echo-type pulse. Assuming a pulse length T, we rescale our variables as follows:

$$\tau = t/T, \quad \omega = \Omega T, \quad k_{ij} = \kappa_{ij}\, T, \quad f(\tau) = w(t/T). \quad (4)$$

The echo pulse shown in Fig. 1 is then given by $f(\tau) = \Theta(1/2 - \tau) - \Theta(\tau - 1/2)$, where $\Theta(t)$ is the Heaviside function. We further define $F(\tau) = \int_0^\tau d\tau' f(\tau') = \tau\Theta(1/2 - \tau) + (1 - \tau)\Theta(\tau - 1/2)$.

According to the ω expansion the leading order (LO) and next-to-leading order (NLO) expressions for the excited state fraction $P_e(\tau)$ are given by

$$P_e^{(\text{LO})}(\tau) = \omega^2 \langle \sigma_{ee}^{i(2)} \rangle = \frac{1}{4}\omega^2 |F(\tau)|^2, \quad (5)$$

$$P_e^{(\text{NLO})}(\tau) = \omega^2 \langle \sigma_{ee}^{i(2)} \rangle + \omega^4 \langle \sigma_{ee}^{i(4)} \rangle = P_e^{(\text{LO})} - \omega^4 (I_{41} + I_{42}), \quad (6)$$

$$I_{41} = \frac{|F(\tau)|^4}{16} - \text{Re}\left[\frac{F(\tau)}{8}\int_0^\tau d\tau_1 f(\tau_1)^* F(\tau_1)^2\right], \quad (7)$$

$$I_{42} = \frac{1}{4}\sum_{i\neq j} \text{Re}\left\{\int_0^\tau d\tau_1 f(\tau_1)[F(\tau) - 2F(\tau_1)] \times \int_0^{\tau_1} d\tau_2 f^*(\tau_2) F^*(\tau_2)[e^{i(\tau_1 - \tau_2)k_{ij}} - 1]\right\}. \quad (8)$$

The Rydberg-Rydberg correlation function is defined by

$$g^{(2)}(i, j) \equiv \frac{\langle \sigma_{ee}^i(\tau)\sigma_{ee}^j(\tau)\rangle}{\langle \sigma_{ee}^i(\tau)\rangle\langle \sigma_{ee}^j(\tau)\rangle}, \quad (9)$$

with leading order approximation in the ω expansion

$$g_{\text{LO}}^{(2)}(i, j) = \frac{4}{|F(\tau)|^4}\left|\int_0^\tau d\tau_1 e^{i\tau_1 k_{ij}} f(\tau_1) F(\tau_1)\right|^2. \quad (10)$$

Calculating higher order corrections to these quantities, although possible in principle, is more tedious than justified. The expressions above can be explicitly evaluated for a homogeneous system with van-der-Waals interaction $\kappa_{ij} = -C_6/|x_i - x_j|^6$. The sum in I_{42} is replaced by $\sum_{i\neq j} \to \int d^3x \rho(x)$, which corresponds to an ensemble average. Throughout the article we write ρ for the full density profile and ρ_0 for the peak density. If we evaluate Eq. (6) at $t = T$ for a homogenous system, we

can obtain the echo signal; that is, the final Rydberg fraction

$$f_e = P_e(T) = \frac{2\omega^4\pi^{3/2}\sqrt{|C_6|}}{2835}(8\sqrt{2}-9)\rho_0. \qquad (11)$$

Other analytical expressions that can be obtained are not illuminating and are therefore omitted here. However, we compare their predictions with direct numerical simulations in Sec. VI. A more detailed description of the ω expansion can be found in Ref. [17].

To estimate which order of the expansion in ω is required for a given scenario, we can consider the excited fraction of a fully blockaded sample of N_b atoms assuming a square pulse:

$$P_e(t) = \frac{1}{N_b}\sin^2(\sqrt{N_b}\Omega t/2) = \sum_n P_e^{(n)}(\Omega t)^n, \qquad (12)$$

which is correctly reproduced by the expansion in the limit of infinite interactions [17]. Roughly knowing the expected N_b for a system and the maximal Ωt, we can estimate how many terms of the series expansion Eq. (12) are required. This will be used in Sec. VI.

III. CORRELATION DYNAMICS

For N_0 atoms homogenously distributed in a cube of volume L^3, we can see that the physics of our problem is governed by two parameters; namely $\omega = \Omega T$ and $U = C_6 T/L^6$. Throughout this article we usually employ $\omega = 0.25$ and $U = -0.0014$. This corresponds, for example, to a ^{87}Rb gas in which states with principal quantum number $n_{\mathrm{Ryd}} = 41$ are excited via a transition with Rabi frequency $\Omega = 2\pi \times 0.1$ MHz during a time of 400 ns. The dimension of the box would be $L = 11$ μm. For these parameters we then vary the number of atoms as listed in Table I, leading to densities of the order of 5×10^{10} cm^{-3}. Compared to the experiment of Ref. [8], these parameters lead to a substantially weaker blockade with maximally about $N_b = 40$ atoms per blockade sphere. This facilitates both the physics of interest here and the numerical simulation. We will use the saturated two-atom blockade radius $r_{b0} = (C_6/\Omega)^{1/6}$ as length scale and express densities using the simple estimate for the blockade volume $V_b = 4\pi r_{b0}^3/3$.

In an echo sequence, we first excite Rydberg states with Rabi frequency Ω for some duration $\tau/2$, followed by a π phase shift of the laser and hence Rabi coupling $-\Omega$ for further time $\tau/2$. These parameters are defined in Sec. II B. For the full quantum dynamics as in Sec. II A, we randomly distribute N_0 atoms, solve the SE and obtain one correlation function defined by Eq. (9) for each pair of atoms. These are binned according to the separation r of those atoms. To minimize finite size effects, we only consider atoms (pairs) inside a central cube of dimension $L/2$ within our simulation volume to calculate N_e [$g^{(2)}$].

In order to obtain a spatial correlation function, we first calculate $g^{(2)}(i,j)$ according to Eq. (9) for each of these atom pairs. We then determine

$$g^{(2)}(r)\sum_{i,j}^{-} g^{(2)}_{i,j}/N(r), \qquad (13)$$

where $\sum^{-}_{i,j}$ denotes a double sum over all atoms that fulfill $|x_i - x_j| \in [r, r+\Delta r)$ for a bin size Δr, and $N(r)$ is the number of atom pairs that fall into each respective bin.

Thus averaging over the entire sample and further over a large number of realizations of the spatial atomic distribution [21], we obtain a spatial correlation function $g^{(2)}(r)$. Our results from numerical solutions [22] of Eq. (2) are shown in Figs. 1 and 2.

Soon after initiating a transfer of atoms to the Rydberg state, the probability to find a pair of excited atoms closer than the sharply defined instantaneous blockade radius $r_b(t)$ is essentially zero. This is due to strong van-der-Waals interactions of those pairs, shifting doubly excited states out of resonance. The radius $r_b(t)$ grows in time, since the longer pulse duration allows an increasingly finer energy resolution. The Rydberg atom number in the echo sequence does not reach the saturation limit, so $r_b(t)$ does not reach its equilibrium extension r_{b0} but continues to grow throughout the excitation

TABLE I. Parameters for the scenarios modeled in this article. In cases (i)–(iii) the atoms are homogeneously distributed in a cubic box of dimension L with periodic boundary conditions [22]. Case (iv) is a Gaussian cloud, as shown, with $\sigma = 1.6 r_{b0}$. This ensures the same peak density as the homogenous density of case (ii). The relevant dimensionless measure of the density is $\rho_0 V_{b0}$. For the parameters described in the text this would correspond to the values in the last row.

Case	(i)	(ii)	(iii)	(iv)
N_0	20	84	125	50
L/r_{b0}	2.5	2.38	2.38	2.38
$\rho_g(r)$	ρ_0	ρ_0	ρ_0	$\rho_0 e^{-2r^2/\sigma^2}$
$\rho_0 V_{b0}$	5.4	26.2	39	26.2
$\rho_0/10^{10}$[cm^{-3}]	1.3	6.3	9.4	6.3

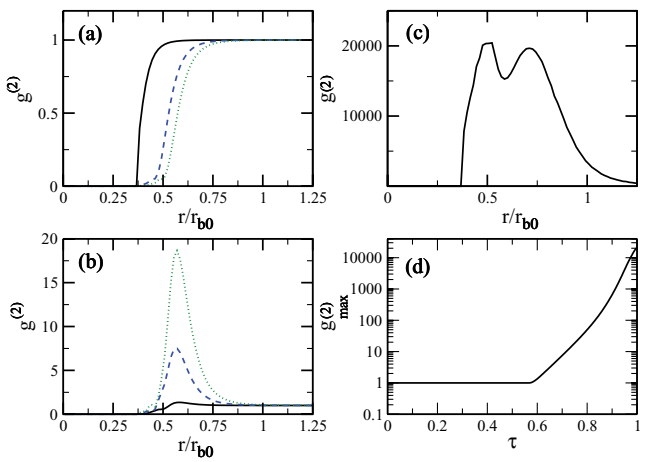

FIG. 2. (Color online) Spatial atomic correlations during an echo sequence with $\rho_0 V_{b0} = 5.4$. (a) Pair correlation function $g^{(2)}(r)$ during the excitation phase at $\tau = 0.05$ (solid black line), $\tau = 0.37$ (blue dashed line) and $\tau = 0.49$ (green dotted line). Below the cutoff length r_{cut}, $g^{(2)}$ is set to zero [22]. (b) The same during the deexcitation phase at $\tau = 0.6$ (solid black line), $\tau = 0.7$ (blue dashed line) and $\tau = 0.75$ (green dotted line). (c) Final shape of the pair correlation function after the pulse ($\tau = 1$). (d) Spatial maximum of pair correlations. The location of the time samples in panels (a)–(c) relative to the pulse can be seen clearly in Fig. 1.

period [Fig. 2(a)]. Following the flip of the phase of the Rabi coupling at $\tau = 0.5$, $g^{(2)}$ develops a dominant peak just outside the blockade radius [Fig. 2(b)]. The height of this peak increases as more and more atoms are transferred back to the ground state [Fig. 2(d)]. Just before the end of the pulse, for densities as low as in Fig. 2, a dip appears in the correlation peak like that shown in Fig. 2(c). This feature starts to occur when the probability for a single excitation in the system drops below that for double excitation.

The underlying physics requires only binary interactions. Consider a pair of atoms separated by some distance r. Let us write the quantum state of this pair as

$$|\Psi\rangle = c_{gg}|g_1 g_2\rangle + c_{eg}|e_1 g_2\rangle + c_{ge}|g_1 e_2\rangle + c_{ee}|e_1 e_2\rangle. \tag{14}$$

Only in the state $|e_1 e_2\rangle$ where both atoms are excited to a Rydberg level do they experience any interaction. The correlation function in state (14) is

$$g^{(2)}(1,2) \equiv \frac{\langle \sigma_{ee}^1(\tau)\sigma_{ee}^2(\tau)\rangle}{\langle \sigma_{ee}^1(\tau)\rangle\langle \sigma_{ee}^2(\tau)\rangle} = \frac{|c_{ee}|^2}{(|c_{eg}|^2+|c_{ee}|^2)(|c_{ge}|^2+|c_{ee}|^2)}. \tag{15}$$

Now consider $g^{(2)}$ after the pulse for three different atomic separations: (i) If the atoms are very close [i.e., $r \lesssim r_b(t)$] double excitation can be considered fully suppressed. Hence $|c_{ee}| = 0$ and $g^{(2)} = 0$. (ii) If the atoms are very far apart the interaction can have no effect. We know then $g^{(2)} = 1$. From Eq. (15) this can be understood since without interactions and for small excited fractions $|c_{ee}| \approx |c_{eg}|^2 = |c_{ge}|^2$ and $|c_{eg}|^2 \gg |c_{ee}|^2$. (iii) In the intermediate range we can neither neglect double excitations nor interaction. Consider the very end of the pulse. The amplitudes c_{eg} and c_{ge} have returned to their initial value of zero after the echo pulse. In contrast $|c_{ee}|$ is nonzero due to the dephasing. We then see that the atomic correlation function scales as $g^{(2)} = 1/|c_{ee}|^2$, which is larger than one.

As shown in Fig. 2, the distances r with pairing correlations during the second half of the pulse are those where correlations change, as r increases, from blockaded [$g^{(2)} = 0$] to uncorrelated [$g^{(2)} = 1$] during the first half of the pulse. We will call the spherical shell around each atom where neighbors have these distances the *partial blockade shell*.

We find that the position of the maximum of the correlation function during the second half of the pulse depends only weakly on time.

IV. SIGNATURES OF PAIRING

In this section we quantify to what extent the correlation dynamics presented in the previous section allow control over the nearest-neighbor distribution in a Rydberg gas. We further discuss observables that are easier to access experimentally than the density-density correlations themselves.

We consider the fraction R of excited atoms separated from their nearest neighbor by a distance in the interval $[r_0, r_0 + d]$,

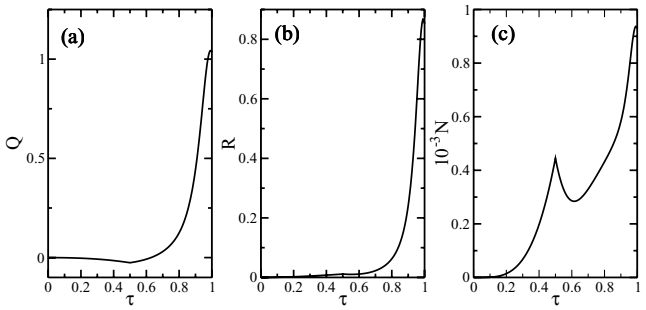

FIG. 3. Visibility of the pairing effect for a density with $\rho V_{b0} = 26.2$. (a) Mandel Q parameter. (b) Fraction R of remnant atoms within the preferred distance peak, using Eq. (16). (c) Total number of paired, excited atoms, extrapolated [24] as if there was a total number of $N_g = 1 \times 10^7$ atoms initially.

chosen to contain the peaks in Fig. 2(a). This is given by

$$R = \frac{\sum_{\mathbf{n}\neq\mathbf{0}} |c_{\mathbf{n}}|^2 f(\mathbf{n})}{\sum_{\mathbf{n}\neq\mathbf{0}} |c_{\mathbf{n}}|^2}, \tag{16}$$

where $f(\mathbf{n})$ is the fraction of excited atoms in the many-body basis state $|\mathbf{n}\rangle$ with at least one excited neighbor in the chosen interval.

For a situation as in Fig. 2, we choose $r_0 = r_{b0}/2$ and $d = r_{b0}/4$. We show in Fig. 3(b) that almost all atoms are paired up before the end of the pulse. In the initial phase, R remains nearly zero owing to the predominance of single excited atoms without neighbors. In Fig. 3(c), we show the total number of paired, excited atoms, obtained by multiplying the paired fraction $R(t)$ by the Rydberg number $N_e(t)$. We then rescale the number obtained, such that it corresponds to a situation with a total initial number of 10^7 atoms, for illustrative purposes. It may seem counter intuitive that the number of paired atoms rises even during the second half of the pulse when atoms are predominantly deexcited. Note, however, that whether or not the Rabi coupling causes excitations or deexcitations depends on the relative populations and phases. The continuous increase of $RN_e(t)$ is again due to interaction-induced decoherence.

Finally, we describe two possibilities to experimentally detect the correlation dynamics:

(i) via the effect of correlations on the number uncertainty in the Rydberg fraction [16] and
(ii) via field ionization of the paired Rydberg atoms.

For case (i), strong deviations from an uncorrelated state have been shown to affect the number statistics of the excited state fraction [7,16]. This is well captured in the Mandel Q parameter [23]

$$Q = \frac{\langle \hat{N}_e^2\rangle - \langle \hat{N}_e\rangle^2}{\langle \hat{N}_e\rangle} - 1 = \int d^3 r \rho_e(r)[g^{(2)}(r) - 1], \tag{17}$$

which can be experimentally determined from the Rydberg atom counting statistics. We show the Q factor in Fig. 3(a). In comparison with the evolution of R, we see that the Q factor becomes large when most Rydberg atoms are paired up. $Q \sim 1$ already represents a sizable deviation of the atom statistics from a Poissonian distribution.

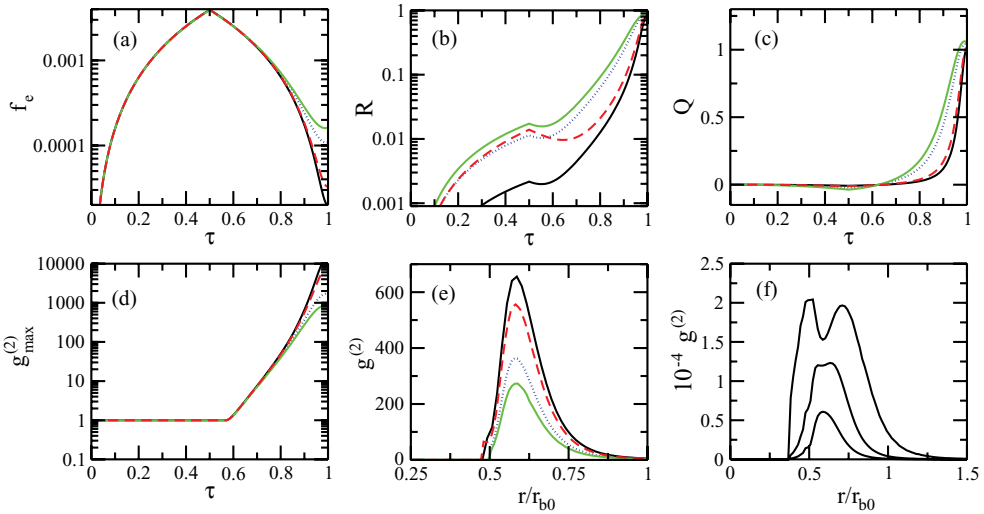

FIG. 4. (Color online) Effects of inhomogeneities and changes of density on the pairing peak. We show densities $\rho_0 V_{b0} = 5.4$, 26.2, 39 as black, blue dotted, and green or gray lines, respectively, and an inhomogeneous case $\rho(x) = \rho_0 \exp(-2r^2/\sigma^2)$ with $\rho_0 V_{b0} = 26.2$ and $\sigma/r_{b0} = 1.6$ (red dashed line). (a) Rydberg fraction f_e; for increasing homogeneous density the final remnant $f_e(\tau = 1)$ gets larger. (b) Paired excited fraction according to Eq. (16). (c) Mandel Q parameter, see Eq. (17). (d) Spatial maximum of pair correlations. (e) $g^{(2)}(r)$ at $\tau = 0.75$, for increasing homogeneous density the peak height decreases. (f) Spatial atomic correlations near the end of an echo pulse in a low-density ($\rho_0 V_{b0} = 5.4$) gas. Shown are snapshots at $\tau = 0.96$, $\tau = 0.98$, and $\tau = 1.0$ in order of increasing peak-height.

For case (ii), the Q factor captures only integrated properties of the correlation function. To obtain information about the spatial shape of atomic correlations after an echo pulse, the paired Rydberg atoms could be field-ionized. The potential energy of the ions due to Coulomb repulsion $E_{\mathrm{Coul}} \approx e^2/(4\pi r_0 \epsilon_0)$ would subsequently be converted into kinetic energy. Since only a small number of atoms occupies Rydberg states, one could hope that the Rydberg fraction is sufficiently dilute for Coulomb scattering to leave the initial kinetic energy distribution essentially unchanged. The peak in the nearest-neighbor distribution function $\sim r^2 g^{(2)}(r)$ then translates into an easily visible maximum of the measured kinetic energy spectrum of the ions. For $\rho V_{b0} = 26.2$, the energy at the maximum is 0.5 meV.

V. VARYING THE SPATIAL ATOMIC DISTRIBUTION

The scenarios shown in the previous section are relatively weakly blockaded and assume a homogeneous distribution of atoms. In this section we study how an inhomogeneous distribution and changes in the overall density affect our results. The basic picture is shown in Figs. 4 and 5. In Fig. 4, we compare a variety of different densities. Prominent features of these data are compared more directly in Fig. 5.

Is is known that the echo signal (i.e., the fraction of Rydberg excitations remaining after the pulse) increases as the density is increased [8]. Using the ω expansion, we can supply the analytical expression Eq. (11) for this increase. For the low densities where it is valid, it performs well, as can be seen in Fig. 5(a). Other effects of increasing density are a decrease of the maximum correlations and an increase of the Mandel Q factor for intermediate times ($\tau \sim 3/4$). Despite the decrease in the correlation peak height, we find that the paired fraction R, defined by Eq. (16), almost reaches unity after the pulse, regardless of the density. This is shown in Fig. 4(e). We also show the development of the dip in the correlation peak in Fig. 4(f). We only see this feature for the lowest densities considered.

The reduction of correlation strength with increasing density can be understood from the nature of the distribution of excitations near the end of the pulse, using only classical arguments. Let us assume a homogenous distribution of pairs of excited atoms within a volume V, with a fixed distance r_0 between the partners of each pair. The distance r_0 then corresponds to the location of our pairing peak, ignoring its finite width. The orientation of pairs in space shall be isotropic. Overall, we thus have a distribution of positions for each pair:

$$f(\mathbf{R}, \mathbf{r}) = \frac{1}{4\pi V} \delta(|\mathbf{r}| - r_0). \tag{18}$$

Here, $\mathbf{R}$ denotes the center-of-mass position of a pair and $\mathbf{r}$ its relative coordinate. Assuming a total number of M pairs we have a pair density $n_p = M/V$ and an excited atom density $n_e = 2M/V$. The positions of the pairs themselves are correlated due to the dipole blockade, we thus assume that the

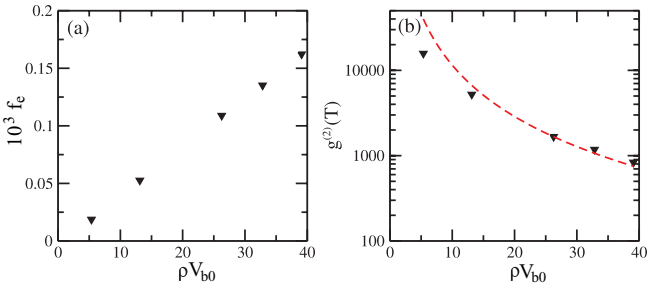

FIG. 5. (Color online) Dependence of echo signal and final correlation peak on atomic density. (a) Final Rydberg fraction at $t = T$. These data are very well described by Eq. (11). (b) (▼) Peak height of $g^{(2)}$ at $t = T$. The red dashed curved shows the functional form $g^{(2)}(\rho) = (\rho_0/\rho)^2 g^{(2)}(\rho_0)$ with reference density $\rho_0 = 26.2$. This is motivated by a simple model explained in the text.

centers of the pairs must be separated by more than a certain radius r_b. The classical correlation function corresponding to our $g^{(2)}$ is

$$\bar{g}^{(2)}(r) = \int d\Omega \frac{E(\mathbf{r_1} = \mathbf{x_0}; \mathbf{r_2} = \mathbf{x_0} + \mathbf{y}, |\mathbf{y}| = r)}{E(\mathbf{r_1} = \mathbf{x_0}) E(\mathbf{r_2} = \mathbf{x_0} + \mathbf{y}, |\mathbf{y}| = r)}. \quad (19)$$

In the numerator, we have the expectation value for the number of joint occupations of the locations r_1 and r_2 by excited atoms. In the denominator, $E(\mathbf{r_1} = \mathbf{x_0})$ denotes the expectation value for the number of excited atoms at location x_0, which is $2M/V$. The integration $d\Omega$ is over the solid angle of orientations of $\mathbf{y}$ with respect to $\mathbf{x_0}$. We are now interested exclusively in the value of the correlation function at the pairing peak, located at $r = r_0$. For simplicity, we assume contributions to the numerator of Eq. (19) stem only from cases where the atoms at both locations were constituents of the same pair. This should be justified when the pairs are sufficiently dilute that their mean distance is much larger than r_0. We can then write $E(\mathbf{r_1} = \mathbf{x_0}; \mathbf{r_2} = \mathbf{x_0} + \mathbf{y}, |\mathbf{y}| = r) = Mf[(\mathbf{r_1} + \mathbf{r_2})/2, \mathbf{r_1} - \mathbf{r_2}]$.

With these simplifying assumptions, we find Eq. (19) equals $V/4M \sim 1/n_p$ for the simple pair distribution described above. Using $n_p \sim n_e$, $n_e = f_e\rho$, and $f_e \sim \rho$ from the ω expansion, we find overall that the correlation strength scales like ρ^{-2}. This behavior is roughly confirmed by the simulation results as shown in Fig. 5(b). It is consistent with a paired fraction R that shows almost no density dependence near the end of the pulse. For each excitation we calculate $N = \int_{r_0}^{r_0+d} r^2 g^{(2)}(r) n_e(r) dr$ to obtain the number of excited neighbors in an interval $[r_0, r_0 + d]$. Since n_e scales like ρ^2 while $g^{(2)}$ scales like ρ^{-2}, we can understand how the final paired fraction can remain almost the same even though the density is varied.

We verified that the relation $g^{(2)}(r_0, \tau) \sim \rho^{-2}$ remains qualitatively unchanged if we model similar echo pulses in a fictitious system with a $1/r^4$ long-range interaction. This lends further support to the simple explanation in terms of the density of available pairs.

Now consider a case with $N_0 = 50$ atoms inhomogeneously distributed with atomic density $\rho(x) = \rho_0 \exp(-2r^2/\sigma^2)$ [case (iv) in Table I]. The peak-density ρ_0 is chosen as for case (ii). Figure 4 includes the correlation function averaged over all atomic pairs in the cloud for this case. It is determined in the same manner as described in Sec. III. One could expect that the inhomogeneity washes out the signal in the correlation function. Instead its visibility is even better than for the homogenous case with equal peak density, owing to the presence of low-density regions in the atomic cloud. For lower density the pairing effect is more prominent, as we already argued. We also do not expect a strong spatial variation of the preferred distance throughout the cloud, since the blockade radius $r_b(t)$ depends only weakly on the atomic density (i.e., the saturated many-body blockade radius scales like $\bar{r}_b \sim \rho_g^{2/5}\Omega$ [6]). Thus, the location of the correlation peak, situated near $r_b(\tau/2)$, is expected to vary only slightly throughout the sample. Consequently, there are only small effects of spatial averaging on the final result in the inhomogeneous case considered here. To fully exclude that density inhomogeneities in an experiment would suppress the signature reported here, one ideally should consider a sample whose width greatly exceeds the characteristic range where the correlation peak is formed ($\sigma \gg r_0$). However, this is computationally intractable.

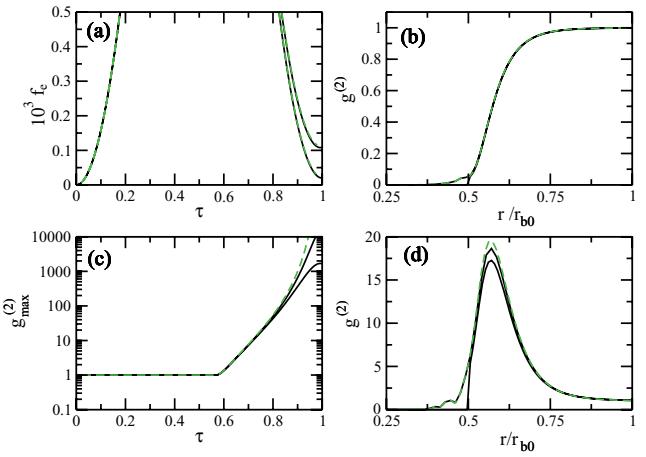

FIG. 6. (Color online) Comparison of the ω expansion (green dashed line) with exact solutions of the SE for $\rho_0 V_{b0} = 5.4$ and $\rho_0 V_{b0} = 26.2$ (solid black line). (a) Excited-state fractions. The higher density case has the higher $f_e(1)$. (b) Pair correlation function $g^{(2)}(r)$ at $\tau = 0.49$. The two cases are almost indistinguishable. (c) Spatial maximum of pair correlations. The higher density case has a lower $g^{(2)}_{\max}(1)$. (d) Pair correlation function $g^{(2)}(r)$ at $\tau = 0.75$. The higher density case has a lower pairing peak and is cutoff at $r = 0.5 r_{b0}$.

VI. COMPARISON WITH ω EXPANSION

The simple expression of Eq. (10) for two-body correlations in the ω expansion does not depend on density and thus cannot capture its effect on correlation dynamics, as shown in Fig. 4. However, for small densities it compares quite well with the substantially more involved exact Schrödinger evolution. This can be expected from Eq. (12) because, for $N_b = 40$, the series is well-described by its first two terms until $\Omega t = 0.25$.

We can see in Figs. 6(a) and 5(a) that the NLO result for the Rydberg fraction [Eq. (6)] gives good quantitative results for the cases considered here. For correlations, we only have the LO expression Eq. (10). We see that this approximation describes correlations in the low density case $\rho_0 V_{b0} = 5.4$ quite well, whereas quantitative deviations appear when the density becomes as high as in the case with $\rho_0 V_{b0} = 26.2$. Qualitative differences in the shape of the correlation function are also present near the very end of the pulse, because Eq. (10) cannot describe the dip seen in Fig. 4(f).

We note that (in particular for cases that show the most dramatic correlation dynamics through an echo pulse), for those cases with a low density, the ω expansion provides useful results.

VII. CONCLUSIONS

We have shown that an echo-type excitation sequence as employed in the experiments of Refs. [8,9] can be used to create Rydberg gases with non-standard nearest-neighbor distribution functions. After the pulse the vast majority of excited atoms possesses a neighbor in a fairly narrow interval around some distance r_0. Variations of the interaction strength

and pulse length can control r_0. The strength of the correlation signal is proportional to ρ^{-2}, where ρ is the atomic density. This can be understood in terms of the quantum state after the echo pulse, independent of the precise form of the interaction.

The described pairing effect in the density-density correlation function is most pronounced for low densities and for gases that are not too strongly blockaded. However, the overall fraction of Rydberg atoms that have a neighbor near the distance r_0 approaches unity regardless of density. Our results were obtained by direct simulation of ensembles of about a hundred atoms. Furthermore, we used these simulations to estimate the range of validity of the first-order approximation of the correlation dynamics obtained using the ω expansion. We find that for weakly blockaded gases it provides useful estimates.

ACKNOWLEDGMENTS

PD was supported by the European Community under the contract MEIF-CT-2006-041390.

[1] M. D. Lukin, M. Fleischhauer, R. Côté, L. M. Duan, D. Jaksch, J. I. Cirac, and P. Zoller, Phys. Rev. Lett. **87**, 037901 (2001).
[2] D. Tong, S. M. Farooqi, J. Stanojevic, S. Krishnan, Y. P. Zhang, R. Côté, E. E. Eyler, and P. L. Gould, Phys. Rev. Lett. **93**, 063001 (2004).
[3] T. A. Johnson, E. Urban, T. Henage, L. Isenhower, D. D. Yavuz, T. G. Walker, and M. Saffman, Phys. Rev. Lett. **100**, 113003 (2008).
[4] K. Singer, M. Reetz-Lamour, T. Amthor, L. G. Marcassa, and M. Weidemüller, Phys. Rev. Lett. **93**, 163001 (2004).
[5] R. Heidemann, U. Raitzsch, V. Bendkowsky, B. Butscher, R. Löw, L. Santos, and T. Pfau, Phys. Rev. Lett. **99**, 163601 (2007).
[6] R. Heidemann, U. Raitzsch, V. Bendkowsky, B. Butscher, R. Löw, and T. Pfau, Phys. Rev. Lett. **100**, 033601 (2008).
[7] T. Cubel Liebisch, A. Reinhard, P. R. Berman, and G. Raithel, Phys. Rev. Lett. **95**, 253002 (2005).
[8] U. Raitzsch, V. Bendkowsky, R. Heidemann, B. Butscher, R. Löw, and T. Pfau, Phys. Rev. Lett. **100**, 013002 (2008).
[9] K. C. Younge and G. Raithel, New J. Phys. **11**, 043006 (2009).
[10] A. Gaëtan, Y. Miroshnychenko, T. Wilk, A. Chotia, M. Viteau, D. Comparat, P. Pillet, A. Browaeys, and P. Grangier, Nature Phys. **5**, 115 (2009).
[11] E. Urban, T. A. Johnson, T. Henage, L. Isenhower, D. D. Yavuz, T. G. Walker, and M. Saffmann, Nature Phys. **5**, 110 (2009).
[12] J. V. Hernandez and F. Robicheaux, J. Phys. B **41**, 195301 (2008).
[13] C. Ates, A. Eisfeld, and J. M. Rost, New J. Phys. **10**, 045030 (2008).
[14] C. Ates, T. Pohl, T. Pattard, and J. M. Rost, Phys. Rev. Lett. **98**, 023002 (2007).
[15] C. Ates, T. Pohl, T. Pattard, and J. M. Rost, Phys. Rev. A **76**, 013413 (2007).
[16] C. Ates, T. Pohl, T. Pattard, and J. M. Rost, J. Phys. B **39**, L233 (2006).
[17] J. Stanojevic and R. Côté (2008), e-print arXiv:0801.2396 [quant-ph].
[18] J. Stanojevic and R. Côté, Phys. Rev. A **80**, 033418 (2009).
[19] H. Weimer, R. Löw, T. Pfau, and H. P. Büchler, Phys. Rev. Lett. **101**, 250601 (2008).
[20] K. C. Younge, A. Reinhard, T. Pohl, P. R. Berman, and G. Raithel, Phys. Rev. A **79**, 043420 (2009).
[21] The number of realizations required for convergence of $g^{(2)}$ ($\tau = 1$) ranged from 500 for case (iii) to 6×10^5 for case (i).
[22] Our simulations use a 8th-9th order adaptive stepsize Runge-Kutta Fehlberg method. The cutoff energy E_{cut} was typically taken as the van der Waals energy of a pair of atoms at a distance $r_{\text{cut}} = r_{b0}/2$, $N_{\max}$ was about 4–6. For case (i), we used $r_{\text{cut}} = 0.38 r_{b0}$. None of the results presented changed upon moderate variation of E_{cut}, $N_{\max}$, the time-step tolerance, or the cubic box dimension L.
[23] L. Mandel, Opt. Lett. **4**, 205 (1979).
[24] To extrapolate, we simply scale the total atom number from 84 to 10^7. This assumes that the simulated cube gives a representative sample of the dynamics of a large homogenous atomic gas.